First-principles calculations of hyperfine parameters with the Gaussian and augmented-plane-wave method: Application to radicals embedded in a crystalline environment

R. Declerck, E. Pauwels, V. Van Speybroeck, and M. Waroquier*
Center for Molecular Modeling, Laboratory of Theoretical Physics, Ghent University, Proeftuinstraat 86, B-9000 Gent, Belgium
(Received 10 August 2006; published 5 December 2006)

A method for the calculation of hyperfine parameters in extended systems under periodic boundary conditions is presented, using the Gaussian and augmented-plane-wave density functional method, and implemented in QUICKSTEP. In order to increase the efficiency in larger systems, a hybrid scheme is proposed, in which an all-electron treatment for the nuclei of interest and a pseudopotential approximation for the remaining atoms in the simulation cell are combined. The method is validated first by comparing the hyperfine parameters for a selection of atoms and small molecules (using a supercell technique) with other theoretical methods and experimental data from literature. As a typical example of a periodic system where our hybrid method can be applied, the hyperfine parameters of the well-characterized *R*2 *L*-α-alanine derived radical are evaluated, yielding results in excellent agreement with the available experimental data.

DOI: 10.1103/PhysRevB.74.245103 PACS number(s): 71.15.−m, 61.72.Bb, 76.30.−v

I. INTRODUCTION

Electron paramagnetic resonance (EPR) is an important spectroscopic tool in the identification of paramagnetic defects. In recent years, there has been a growing interest in the *ab initio* quantum mechanical calculation of these EPR quantities within density functional theory[1,2] (DFT). A recent overview is given in Ref. 3. By comparing the experimental EPR quantities with those computed ab initio from proposed atomic models, it is possible to identify and understand the microscopic structure of these defects.

Three quantities contribute to EPR spectra: (i) the hyperfine parameters (HFP's), (ii) the *g* tensor, and (iii) the zero-field splitting tensor. In this paper we will focus on the first quantity. The HFP's can be computed from the ground state spin density alone, and they probe the spin density of a region near the nucleus. It is therefore imperative to have an accurate description of the spin density at the nuclei and their near vicinity.

Many useful applications of the EPR technique, however, involve paramagnetic defects embedded in crystals and solvents, or—more generally speaking—in condensed systems. Often, these systems are simulated using the pseudopotential (PSP) approximation and periodic boundary conditions. Unfortunately, difficulties arise when evaluating the HFP's within these periodic PSP schemes: (i) the pseudovalence Kohn-Sham (KS) orbitals differ from their all-electron (AE) counterparts within a (predefined) core region and (ii) the core is frozen and effects due to core spin polarization are not included. A solution to the first problem employs the projector augmented wave (PAW) method of Blöchl,[4] either in an AE (frozen-core) approach,[5] or in the PSP approximation combined with a density reconstruction scheme (post-PSP PAW).[6,7] However, as was argued in Ref. 8, these corrections do not solve the problem of the behavior of the exchange-correlation potential in the vicinity of the nucleus, needed for a correct description of spin-polarization effects on the valence orbitals. A solution to both problems was proposed very recently by Yazyev *et al.*,[8] and uses a reconstruction of the AE orbitals and the frozen valence spin-density approximation to solve the KS equations for the core electrons only. This method yields a non-negligible core spin-polarization correction and cancels the largest part of the error induced by the PSP approximation in the reproduction of the isotropic HFP, corresponding to the Fermi contact interaction.

The previous discussion illustrates the need for a hybrid scheme which can perform an AE HFP calculation (using the AE full potential) on those nuclei of interest (this usually involves the paramagnetic defect center itself and the close region around it), and at the same time leaves open the possibility to use the PSP approximation for the remaining atoms in the simulation cell. Most probably, this approximation will not affect the accuracy of the HFP's of interest, because these are determined mainly by the accurate spin density in a region near the nucleus. For this hybrid AE and PSP scheme, we will make use of the Gaussian and augmented-plane-wave density functional method[9–11] (GAPW method), in which the total density is described in a smooth extended part represented in plane waves (PW's), and parts localized close to the nuclei which are expanded in periodic Gaussian functions. The GAPW method exists in both a PSP (Ref. 10) and an AE (Ref. 11) implementation, and both approaches can be easily combined within one simulation. As an AE approach, the GAPW method solves the problems which are inherent to the PSP approximation. Moreover, due to the fact that the GAPW method employs Gaussians, a simulation with an AE treatment for the nuclei of interest requires only a relatively small extra computational cost, while in a pure PW basis set approach, for example, the computational cost would be manifestly higher.

We will elaborate first on the implementation of the HFP's in the GAPW method. Then we will evaluate its accuracy as an AE method, by comparing with other established DFT HFP methods and experimental data from literature for a number of smaller atoms and molecules. Among these DFT methods, we will benchmark against the very recently proposed all-electron mixed-basis (MB) method,[12] which employs a basis set of confined numerical atomic orbitals supplemented with plane waves. Finally, as an instructive

example of an extended system under periodic boundary conditions, our GAPW implementation will be used to calculate the HFP's of the *R*2 *L*-α-alanine radical, for which ample reference data exist. By comparing with the post-PSP PAW method and the cluster in vacuo approach, we will show that there is an excellent agreement with the available experimental results.

II. THEORY

The energy levels and intensities derived from EPR experiments can be reproduced using an effective Hamiltonian, expressed in terms of effective spin operators. This effective Hamiltonian generally consists of three contributions

$$H_{\text{eff}} = \sum_N \mathbf{S} \cdot \mathbf{A}_N \cdot \mathbf{I}_N + \frac{\alpha}{2} \mathbf{B} \cdot \mathbf{g} \cdot \mathbf{S} + \mathbf{S} \cdot \mathbf{D} \cdot \mathbf{S}. \tag{1}$$

$\mathbf{A}_N$ is the hyperfine tensor of rank 2 describing the coupling between the electronic spin $\mathbf{S}$ and the nuclear spin $\mathbf{I}_N$ of a nucleus N. $\mathbf{g}$ is the g tensor which describes the coupling between the electronic spin system and a constant external magnetic field $\mathbf{B}$. $\mathbf{D}$ is the zero-field splitting tensor arising from the magnetic dipolar interactions between multiple unpaired electrons in the system. α represents the fine structure constant and the summation runs over the nuclei. Atomic units are used throughout this paper.

The components of $\mathbf{A}_N$ can be derived from relativistic many-body quantum mechanics, and the most dominant terms are[13,14]

$$A_{N,ij} = A_{\text{iso},N} \delta_{ij} + A_{\text{ani},N,ij}, \tag{2}$$

where

$$A_{\text{iso},N} = \frac{4\pi}{3} \frac{g_e \mu_e g_N \mu_N}{\langle S_z \rangle} \int d\mathbf{r} \rho_s(\mathbf{r}) \delta_T(\mathbf{r}), \tag{3}$$

$$A_{\text{ani},N,ij} = \frac{1}{2} \frac{g_e \mu_e g_N \mu_N}{\langle S_z \rangle} \int d\mathbf{r} \rho_s(\mathbf{r}) \frac{3 r_i r_j - \delta_{ij} r^2}{r^5}. \tag{4}$$

Here, $\rho_s = \rho^\alpha - \rho^\beta$ represents the net electronic spin density, g_e the free-electron g value, μ_e the Bohr magneton, g_N the nuclear gyromagnetic ratio for the nucleus, μ_N the nuclear magneton, $\langle S_z \rangle$ the expectation value of the z component of the total electronic spin, and the vector $\mathbf{r}$ is taken relative to the position of the nucleus. The isotropic HFP A_{iso} corresponds to the Fermi contact interaction, whereas the anisotropic HFP's $A_{\text{ani},ij}$ result from dipole-dipole interactions. The subscripts i,j refer to Cartesian coordinates x, y, and z. Throughout this work, the gyromagnetic ratio data are taken from Ref. 15.

$\delta_T(\mathbf{r})$ is a smeared out δ function which results from scalar relativistic corrections[5,13]

$$\delta_T(\mathbf{r}) \cong \frac{1}{4\pi r^2} \frac{2}{Z\alpha^2} \frac{1}{\left(1 + \frac{2r}{Z\alpha^2}\right)^2}. \tag{5}$$

with Z the atomic number. In the nonrelativistic limit, $\delta_T(\mathbf{r})$ simplifies to a Dirac's delta function.

In the GAPW scheme, the all-electronic density ρ is defined by its expansion in atomic orbitals $\varphi(\mathbf{r})$,

$$\rho(\mathbf{r}) = \sum_{\mu\nu} P_{\mu\nu} \varphi_\mu(\mathbf{r}) \varphi_\nu^*(\mathbf{r}), \tag{6}$$

with $P_{\mu\nu}$ the density matrix. The orbitals $\varphi(\mathbf{r})$ can be further expanded in a set of atom-centered contracted Gaussian basis functions

$$\varphi_\mu(\mathbf{r}) = \sum_a C_{a\mu} g_a(\mathbf{r}), \tag{7}$$

where $g_a(\mathbf{r})$ are the primitive Gaussians.

In an arbitrary way, space is now divided into non overlapping localized spherical regions centered at the nuclei, and the interstitial region. The idea behind the GAPW approach is that the interstitial electronic density varies smoothly and is therefore easily representable in a PW basis, while the rapidly varying density close to the nuclei can be represented in terms of localized functions. The GAPW representation of the density is the sum of three contributions

$$\rho = \tilde{\rho} + \rho^1 - \tilde{\rho}^1. \tag{8}$$

In the soft density $\tilde{\rho}$, the rapid variations of ρ close to the nuclei are removed by putting to zero the coefficients of the most localized Gaussian primitives. Thus, $\tilde{\rho}$ becomes smooth—hence *soft*, as opposed to the real density ρ, which is called *hard*—and is distributed over all space, and can be represented by a relatively small auxiliary basis set of PW's

$$\tilde{\rho}(\mathbf{r}) = \frac{1}{\Omega} \sum_{|\mathbf{G}| < G_C} \tilde{\rho}(\mathbf{G}) e^{i\mathbf{G}\cdot\mathbf{r}}. \tag{9}$$

The other densities

$$\rho^1 = \sum_N \rho_N^1 \quad \text{and} \quad \tilde{\rho}^1 = \sum_N \tilde{\rho}_N^1 \tag{10}$$

are sums of local atom-centered contributions ρ_N^1 and $\tilde{\rho}_N^1$ which are hard and soft, respectively. ρ_N^1 and $\tilde{\rho}_N^1$ are constructed from an expansion of the density ρ and of the soft density $\tilde{\rho}$, respectively, in the primitive orbital basis functions g_a of atom N.

By construction, ρ, $\tilde{\rho}$, ρ_N^1, and $\tilde{\rho}_N^1$ satisfy the following relations:

$$\rho(\mathbf{r}) - \tilde{\rho}(\mathbf{r}) = 0 \quad \text{for } \mathbf{r} \in I, \tag{11}$$

$$\rho_N^1(\mathbf{r}) - \tilde{\rho}_N^1(\mathbf{r}) = 0 \quad \text{for } \mathbf{r} \in I, \tag{12}$$

$$\tilde{\rho}(\mathbf{r}) - \tilde{\rho}_N^1(\mathbf{r}) = 0 \quad \text{for } \mathbf{r} \in U_N, \tag{13}$$

$$\rho(\mathbf{r}) - \rho_N^1(\mathbf{r}) = 0 \quad \text{for } \mathbf{r} \in U_N, \tag{14}$$

where U_N denotes a spherical region around the nucleus N and I the interstitial region outside these atomic regions. Hence, Eq. (8) is fulfilled in all space.

In a spin-unrestricted DFT run, Eqs. (6)–(9) hold for the density in each spin channel, and hence also for the all-electronic spin density ρ_s. Using the GAPW decomposition of the spin density, we have derived expressions for the

evaluation of the hyperfine parameters as follows.

Due to the presence of the δ_T function, we can safely restrict the integration region of the integral in Eq. (3) to U_N, and evaluate the isotropic HFP using the atom-centered density $\rho^1_{s,N}$, which equals the density ρ_s in a region U_N [Eq. (14)]:

$$A_{\mathrm{iso},N} = \frac{4\pi}{3}\frac{g_e\mu_e g_N\mu_N}{\langle S_z\rangle}\int_{\mathbf{r}<U_N} \mathrm{d}\mathbf{r}\rho^1_{s,N}(\mathbf{r})\delta_T(\mathbf{r}). \quad (15)$$

For the calculation of the anisotropic HFP's of nucleus N, we can reorder the GAPW formulation of the spin density as

$$\rho_s = \tilde{\rho}_s + \rho^1_{s,N} - \tilde{\rho}^1_{s,N} + \sum_{M\neq N}(\rho^1_{s,M} - \tilde{\rho}^1_{s,M}). \quad (16)$$

Inserting this expression, together with the PW expansion of the soft spin density $\tilde{\rho}_s$, in Eq. (4), we can evaluate the anisotropic HFP's as

$$\begin{aligned} A_{\mathrm{ani},N,ij} = {} & \frac{1}{2}\frac{g_e\mu_e g_N\mu_N}{\langle S_z\rangle} \\ & \times\left(-\sum_{|\mathbf{G}|<G_C}\frac{4\pi\left(G_iG_j-\frac{1}{3}G^2\delta_{ij}\right)}{G^2}\tilde{\rho}_s(\mathbf{G})\mathrm{e}^{i\mathbf{G}\cdot\mathbf{R}_N}\right. \\ & \left.+\int_{\mathbf{r}<U_N} d\mathbf{r}\left[\rho^1_{s,N}(\mathbf{r})-\tilde{\rho}^1_{s,N}(\mathbf{r})\right]\frac{3r_ir_j-\delta_{ij}r^2}{r^5}\right) \\ & +\Delta A_{N,\mathrm{ani},ij}. \end{aligned} \quad (17)$$

The integration in the third term can be restricted to U_N because Eq. (12) holds. $\Delta A_{N,\mathrm{ani},ij}$ accounts for the small contributions due to the difference $\rho^1_{s,M}-\tilde{\rho}^1_{s,M}$ from neighboring atomic regions

$$\begin{aligned} \Delta A_{\mathrm{ani},N,ij} = {} & \frac{1}{2}\frac{g_e\mu_e g_N\mu_N}{\langle S_z\rangle} \\ & \times\sum_{M\neq N(R_{MN}<R_C)}\int_{\mathbf{r}<U_M} d\mathbf{r}\left[\rho^1_{s,M}(\mathbf{r})-\tilde{\rho}^1_{s,M}(\mathbf{r})\right] \\ & \times\frac{3(r_i+R_{MN,i})(r_j+R_{MN,j})-\delta_{ij}|\mathbf{r}+\mathbf{R}_{MN}|^2}{|\mathbf{r}+\mathbf{R}_{MN}|^5}. \end{aligned} \quad (18)$$

In this equation, the origin of $\mathbf{r}$ is always the geometric position of each nucleus M, and $\mathbf{R}_{MN}=\mathbf{R}_M-\mathbf{R}_N$ is the vector connecting the nuclei M and N. Only nearest-neighboring atomic regions need to be included. This can be controlled by choosing an appropriate maximum value R_C for $R_{MN}=|\mathbf{R}_{MN}|$.

The effect of including augmentation contributions of neighboring sites [Eq. (18)] was estimated to be small.[5] We will elaborate on the impact of Eq. (18) in the next section.

We have implemented this approach, as outlined in Eqs. (15), (17), and (18), into the existing QUICKSTEP[16] code, which is part of the freely available program package CP2K.[17] Efficient integration can be carried out either numerically using atomic Lebedev grids,[18–20] or analytically using the procedures outlined in Refs. 21 and 5.

III. RESULTS AND DISCUSSION

A. Test calculations

The GAPW method for calculating AE HFP's was validated first by comparing the results for a selection of atoms, ions and small molecules with the results from other DFT-based methods, (i) the MB method and (ii) the method[22–24] employed in the GAUSSIAN 03[25] program package (further referred to as the G03 method), as well as with experimental data from literature. In order to sufficiently assess our method, almost the same set of atoms and molecules as in the MB paper have been chosen. To guarantee a fair comparison with the MB results from literature, the local spin density approximation[26] (LSDA) was adopted in a first batch of test calculations. Subsequent tests include PBE (Ref. 27) and BLYP (Refs. 28 and 29) gradient-corrected functionals.

All the isotropic HFP's have been calculated in the nonrelativistic limit, in accordance with the MB and the G03 method. In our method, all atoms, ions, and isolated molecules were approximated by using large supercells of $(25\ \mathrm{a.u.})^3$ The convergence with respect to the size of the supercell has been verified earlier in Ref. 12. We have used the DZVP (Ref. 30) Gaussian type basis set (GAPW and G03), together with a 200 Ry cutoff for the auxiliary PW grid used to represent the soft density $\tilde{\rho}$ (GAPW only). Furthermore, to examine the basis set dependence, several calculations were carried out using the very extended UGBS2P (Ref. 31) Gaussian type basis set.

In Table I, the calculated isotropic HFP's for a selection of isolated atoms and cations are presented. Reassuringly, using the same Gaussian basis set, the GAPW (LSDA/DZVP/200Ry) and the G03 (LSDA/DZVP) results agree to within less than 2% for all species under study. The use of the much larger UGBS2P basis does not systematically lead to a better experimental agreement, and the results of the MB method are still more accurate [mean percentage error (MPE) compared with experiment: 7.6% (DZVP), 6.2% (UGBS2P), and 3.1% (MB)[39]]. The results for the heavier elements $^{87}Sr^+$ and ^{107}Ag are not as good for all theoretical methods, as could be anticipated from the neglect of relativistic effects.[12] In Ref. 12, the authors attribute the overall success of their MB method to the fact that the method employs numerical atomic orbitals as a basis set to describe the molecular orbitals in the regions close to the cores. These atomic orbitals are better suited than Gaussian basis functions to represent the s wave functions at the nuclei, which often dominate the prediction of the isotropic HFP's. This appears to be confirmed in Table I. However, one should not overestimate the qualitative (dis)agreement with experimental results for all methods presented in Table I as the prediction of the isotropic HFP's heavily relies on the details of the calculation such as the choice of the exchange-correlation (XC) functional.[40] This is shown in Table II, where we have computed the isotropic HFP's for the same set of atoms and cations. Using LSDA, BLYP, and PBE XC functionals, respectively, the predictions for each element vary in a range of as much as 19% (8.9% on average) of the experimental value, and no XC functional is found to be superior to the other.

In Table III, the HFP's of zinc complexes ^{67}ZnX are shown. They provide a more relevant test than atomic calcu-

TABLE I. Comparison of isotropic HFP's (in MHz) for a selection of isolated atoms and ions.

Atom	G03[a] LSDA/DZVP	GAPW[a] LSDA/DZVP/200Ry	GAPW[a] LSDA/UGBS2P/200Ry	MB[b] LSDA/200Ry	Expt.[c]
^{1}H	1362.6	1353.8	1344.5		1420.4
^{7}Li	382.7	380.0 (400.2[d])	395.6	401.6	401.7
^{25}Na	905.7	891.2	974.3	891.2	885.8
^{25}Mg^{+}	−541.5	−538.0	−619.6	−600.2	±596.2
^{39}K	242.1	236.8	241.5	232.4	230.9
^{43}Ca^{+}		−721.5	−813.8	−812.8	±806.4
^{63}Cu	6000.9	5971.3	5944.8	5935.1	5867
^{87}Sr^{+}	−829.0	−820.1	−899.2	−912.7	990−1000.5
^{107}Ag	−1339.0	−1326.7	−1344.9	−1411.3	−1713

[a]Present work.
[b]MB results from Ref. 12.
[c]Experimental data from Ref. 32 (^{1}H), Ref. 33 (^{7}Li, ^{25}Na, ^{39}K), Ref. 34 (^{63}Cu), Ref. 35 (^{107}Ag), Ref. 36 (^{25}Mg^{+}), Ref. 37 (^{43}Ca^{+}), and Ref. 38 (^{87}Sr^{+}).
[d]Using the *Montreal* variant of the DZVP basis set.

lations, mainly because they also allow us to evaluate the accuracy of the anisotropic HFP results. In Table III, the anisotropy is formulated concisely as $A_{\mathrm{ani}}=A_{\mathrm{ani},\parallel}-A_{\mathrm{ani},\perp}$, the difference between the parallel and the orthogonal principal components of the anisotropic HFP matrix. Due to the absence of reliable experimental data, we benchmarked against the results from two-component scalar relativistic zero-order-regular-approximation (ZORA) calculations.[41] All HFP calculations, including those in the MB method, were performed within the LSDA using the geometries from Ref. 41. We again obtain a good agreement between the GAPW (LSDA/DZVP/200Ry) and the G03 (LSDA/DZVP) results, as should be the case. For the isotropic HFP's, all presented methods perform about equally well, with the exception of ^{107}Ag, where all methods seem to fail due to relativistic effects as mentioned above. For the anisotropic HFP's, however, the MB method performs worse than other methods [MPE from ZORA results: 4.1% (DZVP), 6.8% (UGBS2P), and 26.8% (MB)[43]]. Further investigation is needed to determine exactly why the MB results deviate for this set of zinc complexes.

In order to quantify the effect the inclusion of $\Delta A_{\mathrm{ani},N,ij}$ [Eq. (18)] in the calculation of the anisotropic HFP's using the GAPW method, we have extended the test set to methyl, silyl, and germyl radicals. In these molecules, the unpaired electron is mainly localized around the central ^{13}C/^{29}Si/^{73}Ge nucleus, and therefore it is likely that the prediction of the anisotropic HFP's for the nearby ^{1}H nuclides will suffer from the difference $\rho_s^1-\tilde{\rho}_s^1$ in the C/Si/Ge region $U_{\mathrm{C/Si/Ge}}$. From Table IV, it is clear that the inclusion of Eq. (18) does not affect the anisotropic HFP's for ^{13}C/^{29}Si/^{73}Ge at all [0.0% percentage error from the results with Eq. (18)], as was to be expected, while the ^{1}H anisotropic HFP's differ to a small but pronounced extent [percentage error from the results with Eq. (18): 15.0% max, 4.2% mean].

B. The *R*2 *L*-α-alanine derived radical

The real application field of the GAPW HFP method undoubtedly lies in the prediction of HFP parameters of paramagnetic defects in extended periodic systems, like a crystal. Therefore, we have chosen to calculate the HFP's of the

TABLE II. Dependence of isotropic HFP's from the species of Table I on the XC functional (in MHz).

Atom	GAPW[a,b] LSDA/UGBS2P/200Ry	GAPW[a] BLYP/UGBS2P/200Ry	GAPW[a] PBE/UGBS2P/200Ry	Expt.[b]
^{1}H	1344.5	1495.7	1462.3	1420.4
^{7}Li	395.6	460.4	384.0	401.7
^{25}Na	974.3	1002.5	893.9	885.8
^{25}Mg^{+}	−619.6	−629.0	−593.8	±596.2
^{38}K	241.5	239.1	213.4	230.9
^{43}Ca^{+}	−813.8	−806.7	−762.1	±806.4
^{63}Cu	5944.8	5846.0	5699.0	5867
^{87}Sr^{+}	−899.2	−886.8	−844.3	990−1000.5
^{107}Ag	−1344.9	−1298.0	−1278.0	−1713

[a]Present work.
[b]See Table I.

TABLE III. HFP's (in MHz) for zinc complexes. In this table, $A_{ani}=A_{ani,\parallel}-A_{ani,\perp}$.

		Zn part		*X* part	
Zn*X*	Method	A_{iso}	A_{ani}	A_{iso}	A_{ani}
$^{67}Zn^{107}Ag$	G03 DZVP[a]	315.3	20.7	−988.4	−0.7
	GAPW DZVP[a]	315.1	20.4	−979.2	−0.7
	GAPW UGBS2P[a]	303.0	24.1	−981.1	−0.4
	MB[b]	333.2	26.5	−1051.4	−0.1
	ZORA[c]	357	21	−1297	−1
	Expt.[d]			−1324	0
$^{67}Zn^{1}H$	G03 DZVP[a]	553.7	66.2	540.8	−2.2
	GAPW DZVP[a]	538.3	66.0	551.8	−2.4
	GAPW UGBS2P[a]	547.2	67.2	477.7	−2.0
	MB[b]	549.2	74.1	468.5	−1.3
	ZORA[c]	561	63	543	0
	Expt.[d]			486	−2
$^{67}Zn^{13}CN$	G03 DZVP[a]	1019.0	53.2	277.1	35.1
	GAPW DZVP[a]	1012.9	52.9	281.5	35.1
	GAPW UGBS2P[a]	1003.8	54.8	238.2	36.3
	MB[b]	980.1	64.4	258.4	23.1
	ZORA[c]	1044	53	253	38
	Expt.[d]				
$^{67}Zn^{19}F$	G03 DZVP[a]	1179.9	42.5	353.4	827.1
	GAPW DZVP[a]	1169.8	42.3	363.8	834.2
	GAPW UGBS2P[a]	1188.4	39.7	247.2	774.0
	MB[b]	1151.6	60.5	196.2	822.6
	ZORA[c]	1223	40	235	866
	Expt.[d]			129	816

[a]Present work.
[b]MB results from Ref. 12.
[c]ZORA results from Ref. 41.
[d]Experimental results from Ref. 42.

L-α-alanine *R*2 radical (see Fig. 1), which has been well-characterized through experimental and theoretical studies. The amino acid alanine is widely used as a dosimetric system in the solid state, due to a number of valuable radiation dosimetric properties (Refs. 44–46, and references therein). As determined by Sagstuen *et al.*[47] (at room temperature) using a combination of EPR techniques, three radical species are generated within the solid state matrix following irradiation, and two of them are most abundant: *R*1[$C^{\bullet}H(CH_3)COOH$] and *R*2[$N^{+}H_3C^{\bullet}(CH_3)COO^{-}$]. *R*2 is by far the simplest system, as it differs from undamaged alanine only by one hydrogen atom.

Following the experimental characterization of the radiation-induced species in this amino acid, several theoretical studies have been performed with the intent of modeling the radical structures and simulating the corresponding EPR properties. Ban *et al.*[48] and Lahorte *et al.*[49] both used variations of a single molecule approach to calculate the HFP's of alanine radicals. Pauwels *et al.*[50] adopted both cluster in vacuo and periodic approaches to model the alanine *R*2 radical. The explicit incorporation of intermolecular interactions proved essential in the determination of a reliable radical geometry and the subsequent HFP calculations on the single radical.

TABLE IV. Anisotropic HFP's (in MHz) for CH_3, SiH_3, and GeH_3. Calculations were performed in the LSDA, using DZVP basis sets.

Mol.	Nucl.		GAPW w Eq. (18)	GAPW w/o Eq. (18)	pct. error (%)
$^{13}C^{1}H_3$	^{13}C	$A_{ani,\perp}$	−77.2	−77.1	0.0
		$A_{ani,\parallel}$	154.3	154.3	0.0
	^{1}H	$A_{ani,xx}$	−38.0	−37.9	0.2
		$A_{ani,yy}$	−1.6	−1.6	1.4
		$A_{ani,zz}$	39.7	39.5	0.5
$^{29}Si^{1}H_3$	^{29}Si	$A_{ani,\perp}$	86.0	86.0	0.0
		$A_{ani,\parallel}$	−172.0	−172.0	0.0
	^{1}H	$A_{ani,xx}$	−9.9	−9.6	2.8
		$A_{ani,yy}$	1.3	1.5	15.0
		$A_{ani,zz}$	8.7	8.1	6.4
$^{73}Ge^{1}H_3$	^{73}Ge	$A_{ani,\perp}$	41.9	41.9	0.0
		$A_{ani,\parallel}$	−83.9	−83.9	0.0
	^{1}H	$A_{ani,xx}$	−12.1	−11.9	1.7
		$A_{ani,yy}$	4.4	4.6	4.2
		$A_{ani,zz}$	7.7	7.3	5.9

In this section, we will compare a GAPW periodic HFP calculation on the *R*2 radical with a cluster in vacuo approach and a post-PSP PAW periodic HFP calculation. In the GAPW calculation, we will use an AE treatment for the central *R*2 radical and a PSP treatment for the alanine molecules (denoted as AE+PSP), which is an example of the hybrid AE and PSP scheme mentioned in the Introduction.

In the cluster in vacuo approach, a cluster similar to the one in Ref. 50 was adopted. Radical *R*2 was sur-

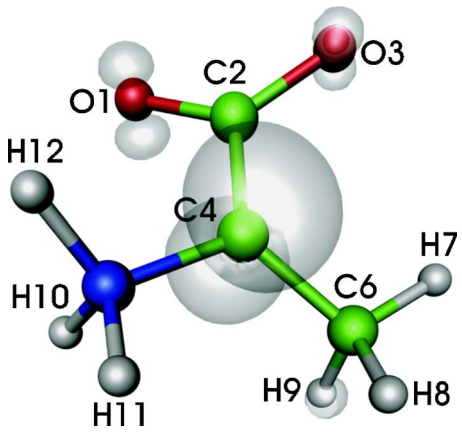

FIG. 1. (Color online) The *R*2 radical geometry, together with an isosurface plot of the spin density (ρ_s=0.01).

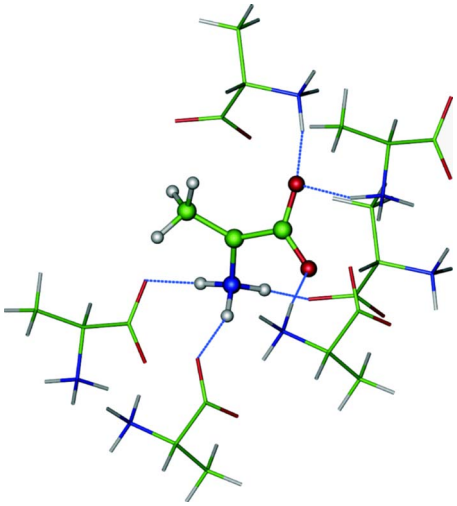

FIG. 2. (Color online) Optimized cluster in vacuo model geometry of the *R*2 radical and its neighboring *L*-α-alanine molecules.

rounded by six alanine molecules in accordance with the space group symmetry of the *L*-α-alanine crystal, which features unit cell constants of $a=11.386$ a.u., $b=23.289$ a.u., $c=10.928$ a.u.[51] This cluster comprises all molecules that are engaged in hydrogen bonds with the central radical. The structure of this hydrogen-bond cluster in vacuo model is shown in Fig. 2. Using GAUSSIAN 03, geometry optimizations were performed on the central radical, while keeping the coordinates of the surrounding alanine molecules fixed in space at the geometry of the crystal structure. Contrary to the original approach by Pauwels *et al.*,[50] the HFP's were calculated using the full cluster, in accordance with the methodology of Ref. 52.

In the periodic boundary model, we doubled the unit cell in the a and c direction, to ensure that neighboring radicals are well separated from each other. The resulting orthorhombic simulation cell contains 15 *L*-α-alanine molecules and a central *R*2 radical, as is shown in Fig. 3. All atoms were free to relax during the geometry optimization, performed with QUICKSTEP.

For the cluster in vacuo model, we employed a TZVP (Ref. 30) basis set for the entire cluster. In the periodic boundary model, we used the same TZVP basis set for the central radical, and a TZVP-PSP (Ref. 53) basis set and pseudopotentials of Goedecker and co-workers[54,55] for the alanine molecules. A BLYP gradient-corrected functional was used throughout all calculations. The post-PSP PAW[6] HFP calculation was performed with the CPMD program package,[56] using the geometry obtained with QUICKSTEP. In this calculation, we used Troullier-Martins[57] (TM) norm-conserving PSP's at a PW cutoff value of 100 Ry. We have also performed a GAPW HFP calculation using an AE treatment for the entire system, but this did not significantly alter the results obtained using the hybrid AE+PSP GAPW method.

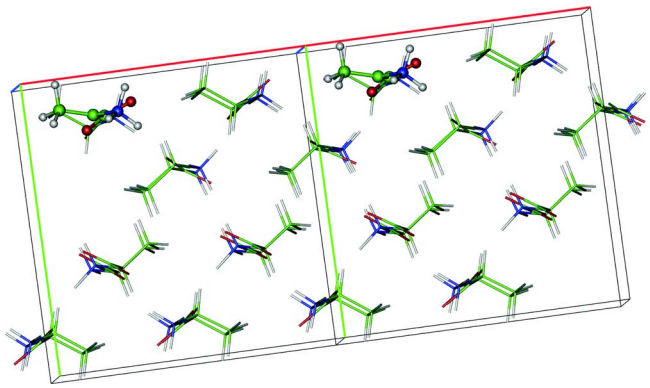

FIG. 3. (Color online) Optimized periodic boundary geometry of the *R*2 radical and its neighboring *L*-α-alanine molecules. The simulation cell and one of its neighboring images are shown.

The calculated HFP's of the *R*2 radical are presented in Table V, along with an overview of the available experimental data, measured at room temperature.[47] The numbering of the nuclei is defined in Fig. 1. Since the methyl group is a quasifree rotor at this temperature, only averaged HFP's have been measured. All of our calculations are static though (formally at 0 K) and do not explicitly take into account this rotational averaging. Nevertheless, to allow for comparison, the hyperfine tensors of H7, H8, and H9 have been averaged (denoted as H7-9 in Table V).

Comparing the calculated HFP's with the available experimental data, all three methods are found to perform very well. Isotropic HFP's deviate 5 MHz at most, and the anisotropic HFP's are also quite accurately reproduced. Larger variations among the calculated HFP's are observed for the nuclei O1-C6, but no experimental information is available to assess these results.

The angular differences between experimental and calculated principal directions are denoted between brackets in Table V. For all directions corresponding to the maximum anisotropic HFP, all angles are well below 10°, indicating an excellent agreement with experiment. For the small and intermediate anisotropic interactions, the agreement is somewhat less. The mutual occurrence of rather large angles for both minor anisotropic interactions can be ascribed to the quasidegeneracy of these interactions, rendering them quite sensitive.

Both methods employing periodic boundary conditions are superior to the cluster in vacuo model, which, for instance, shows the largest angular deviations from experiment, and the least accurate anistropic HFP's. This presumably reflects the limited inclusion of the solid-state environment in this model. Furthermore, the cluster in vacuo model necessitates constraints on the molecules surrounding the radical, and cluster size effects can cause errors. Periodic boundary calculations are clearly a more natural way of simulating the solid state.

The hybrid GAPW HFP method introduced in this work edges out the post-PSP PAW method, as the former results in an impressive agreement with the experimental results of Sagstuen *et al.*, both for (an)isotropic HFP's and for the principal directions.

IV. CONCLUSION AND OUTLOOK

We have proposed a method for the calculation of AE HFP's in extended systems under periodic boundary condi-

TABLE V. HFP's for the *R*2 radical. The values between brackets denote the angles (in degrees) between the calculated and the experimental principal directions.

	GAPW AE+PSP[a] BLYP/TZVP/200Ry				post-PSP PAW[a] BLYP/PW/100Ry				G03[a] BLYP/TZVP				Expt.[b]			
	A_{iso}	$A_{ani,xx}$	$A_{ani,yy}$	$A_{ani,zz}$	A_{iso}	$A_{ani,xx}$	$A_{ani,yy}$	$A_{ani,zz}$	A_{iso}	$A_{ani,xx}$	$A_{ani,yy}$	$A_{ani,zz}$	A_{iso}	$A_{ani,xx}$	$A_{ani,yy}$	$A_{ani,zz}$
O1	−5.3	−31.5	14.4	17.1	−20.0	−32.5	14.6	17.9	−12.1	−31.2	14.4	16.8				
C2	−29.2	−2.1	−1.5	3.6	−30.9	−3.1	−1.2	4.2	−23.9	−2.0	−1.0	3.0				
O3	−2.9	−23.2	11.0	12.2	−13.8	−24.1	11.2	12.8	−6.9	−21.7	10.0	11.7				
C4	87.6	−71.9	−70.8	142.8	237.1	−82.0	−80.9	162.9	129.3	−70.5	−69.4	139.9				
N5	−3.6	−1.2	−0.9	2.1	−2.2	−1.3	−1.1	2.4	−3.1	−0.7	−0.6	1.3				
C6	−27.0	−3.0	0.7	2.3	−25.8	−3.1	0.4	2.7	−23.6	−3.4	−0.2	3.6				
H7	129.8	−5.0	−2.8	7.8	120.2	−5.2	−3.4	8.6	81.5	−4.5	−3.0	7.5				
H8	9.2	−4.2	−3.4	7.5	9.0	−4.5	−3.5	8.0	5.0	−3.7	−3.4	7.2				
H9	71.8	−4.8	−3.0	7.8	66.2	−5.2	−3.2	8.5	127.6	−5.7	2.6	8.3				
H7-9	70.2	−2.8	−2.3	5.1	65.1	−2.9	−2.3	5.2	71.4	−2.6	−1.9	4.5	70.8	−2.9	−2.7	5.6
		(5.0°)	(4.5°)	(2.2°)		(5.4°)	(4.9°)	(2.4°)		(47.6°)	(47.9°)	(5.1°)				
H10	87.7	−6.1	−2.5	8.5	81.8	−6.2	−2.9	9.1	84.9	−5.4	−2.9	8.3	86.3	−6.9	−2.7	9.5
		(2.6°)	(1.0°)	(2.5°)		(3.2°)	(3.4°)	(2.8°)		(14.0°)	(15.1°)	(8.3°)				
H11	10.9	−5.0	−4.5	9.5	10.5	−5.4	−4.5	9.9	7.3	−4.5	−4.3	8.8	10.2	−4.9	−4.8	9.7
		(45.6°)	(45.6°)	(0.8°)		(25.6°)	(25.6°)	(0.9°)		(27.3°)	(27.4°)	(4.0°)				
H12	26.0	−5.8	−4.2	10.0	23.9	−6.2	−4.3	10.5	27.4	−5.3	−4.3	8.8	30.2	−6.1	−4.7	10.7
		(0.5°)	(0.3°)	(0.5°)		(8.5°)	(8.5°)	(1.5°)		(8.9°)	(7.4°)	(5.7°)				

[a]Present work.
[b]Experimental results from Ref. 47.

tions, using the GAPW method. We have implemented this method in QUICKSTEP. The method was validated first by comparing the results for a selection of atoms and small molecules (using a supercell technique) with other theoretical and experimental data. Here, we have also quantified the impact of the inclusion of augmentation contributions from neighboring atomic sites. We have proposed a hybrid AE and PSP scheme, a combination of an AE treatment for the nuclei of interest and a PSP approximation for the remaining atoms in the simulation cell. Using the *R*2 *L*-α-alanine derived radical as an example, we then showed that this hybrid scheme results in relatively inexpensive yet highly accurate HFP calculations in an extended periodic system. In combination with the molecular dynamics capabilities of the CP2K program package, we plan to use our method for hyperfine parameter studies at finite temperatures.

ACKNOWLEDGMENTS

This work was supported by the Fund for Scientific Research–Flanders and the Research Board of Ghent University.

*Electronic address: Michel.Waroquier@UGent.be

[1] P. Hohenberg and W. Kohn, Phys. Rev. **136**, B864 (1964).
[2] W. Kohn and L. Sham, Phys. Rev. **140**, A1133 (1965).
[3] M. Kaupp, M. Bühl, and V. G. Malkin, *Calculations of NMR and EPR parameters: Theory and Applications* (Wiley-VCH, Weinheim, 2004).
[4] P. E. Blöchl, Phys. Rev. B **50**, 17953 (1994).
[5] P. E. Blöchl, Phys. Rev. B **62**, 6158 (2000).
[6] C. G. Van de Walle and P. E. Blöchl, Phys. Rev. B **47**, 4244 (1993).
[7] G. Csányi and T. A. Arias, Chem. Phys. Lett. **360**, 552 (2002).
[8] O. V. Yazyev, I. Tavernelli, L. Helm, and U. Röthlisberger, Phys. Rev. B **71**, 115110 (2005).
[9] G. Lippert, J. Hutter, and M. Parrinello, Mol. Phys. **92**, 477 (1997).
[10] G. Lippert, J. Hutter, and M. Parrinello, Theor. Chem. Acc. **103**, 124 (1999).
[11] M. Krack and M. Parrinello, Phys. Chem. Chem. Phys. **2**, 2105 (2000).
[12] M. S. Bahramy, M. H. F. Sluiter, and Y. Kawazoe, Phys. Rev. B **73**, 045111 (2006).
[13] S. Blügel, H. Akai, R. Zeller, and P. H. Dederichs, Phys. Rev. B **35**, 3271 (1987).
[14] J. E. Harriman, *Theoretical Foundations of Electron Spin Resonance* (Academic Press, New York, 1978).
[15] D. M. Granty and R. K. Harris, *Encyclopedia of Nuclear Mag-*

netic Resonance (Wiley, Chichester, UK, 1996), Vol. 5.
[16] J. VandeVondele, M. Krack, F. Mohamed, M. Parrinello, T. Chassaing, and J. Hutter, Comput. Phys. Commun. **167**, 103 (2005).
[17] http://cp2k.berlios.de.
[18] V. I. Lebedev, Zh. Vychisl. Mat. Mat. Fiz. **15**, 48 (1975).
[19] V. I. Lebedev, Zh. Vychisl. Mat. Mat. Fiz. **16**, 293 (1976).
[20] V. I. Lebedev, Sib. Math. J. **15**, 48 (1977).
[21] H. M. Petrilli, P. E. Blöchl, P. Blaha, and K. Schwarz, Phys. Rev. B **57**, 14690 (1998).
[22] R. F. Curl Jr., Mol. Phys. **9**, 585 (1965).
[23] J. Gauss, K. Ruud, and T. Helgaker, J. Chem. Phys. **105**, 2804 (1996).
[24] V. Barone, Chem. Phys. Lett. **262**, 201 (1996).
[25] M. J. Frisch *et al.*, *Gaussian 03, Revision D.01*, Gaussian, Inc., Wallingford, CT, 2004.
[26] J. P. Perdew and A. Zunger, Phys. Rev. B **23**, 5048 (1981).
[27] J. P. Perdew, K. Burke, and M. Ernzerhof, Phys. Rev. Lett. **77**, 3865 (1996).
[28] A. D. Becke, Phys. Rev. A **38**, 3098 (1988).
[29] C. Lee, W. Yang, and R. G. Parr, Phys. Rev. B **37**, 785 (1988).
[30] N. Godbout, D. R. Salahub, J. Andzelm, and E. Wimmer, Can. J. Chem. **70**, 560 (1992).
[31] E. V. R. de Castro and F. E. Jorge, J. Chem. Phys. **108**, 5225 (1998).
[32] L. Wilmer Anderson, F. M. Pipkin, and J. C. Baird, Phys. Rev. **120**, 1279 (1960).
[33] G. H. Fuller and V. W. Cohen, Nucl. Data, Sect. A **5**, 433 (1969).
[34] Y. Ting and H. Lew, Phys. Rev. **105**, 581 (1957).
[35] G. Wessel and H. Lew, Phys. Rev. **92**, 641 (1953).
[36] C. Sur, B. K. Sahoo, R. K. Chaudhuri, B. P. Das, and D. Mukherjee (unpublished).
[37] B. K. Sahoo, R. K. Chaudhuri, B. P. Das, S. Majumder, H. Merlitz, U. S. Mahapatra, and D. Mukherjee, J. Phys. B **36**, 1899 (2003).
[38] A.-M. Mårtensson-Pendrill, J. Phys. B **35**, 917 (2002).
[39] In these figures, the predictions for ^{1}H and ^{87}Sr were omitted.
[40] *Calculation of NMR and EPR parameters: Theory and Applications*, edited by M. Kaupp, M. Bühl, and V. G. Malkin (Wiley-VCH, Weinheim, 2004).
[41] P. Belanzoni, E. van Lenthe, and E. J. Baerends, J. Chem. Phys. **114**, 4421 (2001).
[42] W. Weltner, *Magnetic Atoms and Molecules* (Van Nostrand Reinhold, New York, 1983).
[43] In these figures, the predictions for ^{107}Ag and ^{1}H were omitted.
[44] E. Malinen, M. Z. Heydari, E. Sagstuen, and E. O. Hole, Radiat. Res. **159**, 23 (2003).
[45] D. Regulla, Appl. Radiat. Isot. **52**, 1023 (2000).
[46] V. Gancheva, E. Sagstuen, and N. D. Yordanov, J. Phys. Chem. **75**, 329 (2006).
[47] E. Sagstuen, E. O. Hole, S. R. Haugedal, and W. H. Nelson, J. Phys. Chem. A **101**, 9763 (1997).
[48] F. Ban, S. D. Wetmore, and R. J. Boyd, J. Phys. Chem. A **103**, 4303 (1999).
[49] P. Lahorte, F. De Proft, G. Vanhaelewyn, B. Masschaele, P. Cauwels, F. Callens, P. Geerlings, and W. Mondelaers, J. Phys. Chem. A **103**, 6650 (1999).
[50] E. Pauwels, V. Van Speybroeck, P. Lahorte, and M. Waroquier, J. Phys. Chem. A **105**, 8794 (2001).
[51] M. S. Lehmann, T. F. Koetzle, and W. C. Hamilton, J. Am. Chem. Soc. **94**, 2657 (1972).
[52] E. Pauwels, V. Van Speybroeck, and M. Waroquier, J. Phys. Chem. A **108**, 11321 (2004).
[53] G. Lippert, J. Hütter, P. Ballone, and M. Parrinello, J. Phys. Chem. **100**, 6231 (1996).
[54] S. Goedecker, M. Teter, and J. Hutter, Phys. Rev. B **54**, 1703 (1996).
[55] C. Hartwigsen, S. Goedecker, and J. Hutter, Phys. Rev. B **58**, 3641 (1998).
[56] CPMD, version 3.11.1, Copyright IBM Corp. 1990-2006, Copyright MPI für Festkörperforschung Stuttgart 1997-2001; http://www.cpmd.org
[57] N. Troullier and J. L. Martins, Phys. Rev. B **43**, 1993 (1991).